Journal of Innovative Optical Health Sciences
Vol. 4, No. 2 (2011) 165−171

DOI: 10.1142/S1793545811001344

IN VIVO VALIDATION OF DUAL-MODALITY SYSTEM FOR SIMULTANEOUS POSITRON EMISSION TOMOGRAPHY AND OPTICAL TOMOGRAPHIC IMAGING

XIN WANG*, BIN ZHANG*, XU CAO*, FEI LIU*,
SHUANGQUAN LIU†, BAOCI SHAN† and JING BAI*,‡
*Department of Biomedical Engineering, Tsinghua University
Beijing, 100084, China

†Key Laboratory of Nuclear Analytical Techniques
Institute of High Energy Physics
Chinese Academy of Sciences, Beijing, 100049, China
‡deabj@mail.tsinghua.edu.cn

We report on tests of combined positron emission tomography (PET) and fluorescence molecular tomography (FMT) imaging system for *in vivo* investigation on small animals. A nude mouse was inoculated with MD-MB-231 breast cancer cells which expressed red fluorescent protein (RFP). For FMT system, reflective illumination mode was adopted with full-angle data acquisition. [18F]-Fluorodeoxyglucose ([18F]-FDG) was used as radioactive tracer for PET. Both data were acquired simultaneously and then reconstructed separately before fusion. Fluorescent tomography results showed exactly where the tumor was located while PET results offered more metabolic information. Results confirmed feasibility for tumor detection and showed superiority to single modality imaging.

Keywords: Dual-modality imaging; positron emission tomography; fluorescence molecular tomography.

1. Introduction

Multimodality imaging has become a research hotspot because it can harness the strengths of different imaging modalities and offer complementary information effectively. A variety of multimodality strategies are available for small animal studies such as positron emission tomography/magnetic resonance imaging (PET/MRI) and microcomputed tomography/single photon emission computed tomography (CT/SPECT) with which we can acquire anatomical and functional information simultaneously.[1,2]

In recent years, molecular imaging, which can visualize and characterize biological processes at the cellular and molecular level within intact living organisms, has attracted many researchers' attention.[3] At present the main molecular imaging methods are PET and optical imaging. PET, by labeling biomolecules with radionuclide to offer metabolic information, is an established molecular and functional imaging technology widely used in clinical examinations. Fluorescence molecular tomography (FMT) is an optical imaging method that has developed rapidly in recent years. It can acquire 3D location of fluorescent dyes. The development of free-space complete angle projection system for FMT, further improved the resolution and sensitivity.[4]

Now, it has become an efficient tool widely used in biomedical research.

To acquire more molecular and functional information, many researchers take advantage of both the molecular imaging methods. Autiero and colleagues first proposed an optical and radionuclide planar imaging system.[5] With this system, 2D fluorescent and radioactive information could be acquired simultaneously. Prout and colleagues designed a combined detector named OPET, capable of acquiring PET and optical signals in turns.[6] For this system, small animals are required to abut the inside surface of the detectors, which was not convenient in practice. Peter and colleagues reported a dual-modality positron/optical small animal tomographic imaging instrument, which used thin complementary metal oxide semiconductor (CMOS) chips inside a circular PET detector as fluorescence detectors. However, its optical sensitivity was lower contrasted with a charged-coupled device (CCD) camera.[7]

Different from the systems introduced above, we designed a dual-modality system with which 3D radioactive and fluorescent information can be acquired simultaneously. Description of the prototype for fluorescence and radionuclide imaging system has been reported in a previous paper[8] in which, indocyanine green (ICG) was used as fluorescent probe for *in vivo* experiments. However, ICG probes can not indicate where the tumor is located. To further validate the feasibility and performance of this combined system for tumor detection, we performed *in vivo* experiments as follows. Red fluorescent protein (RFP) expressing tumor cells were injected into a nude mouse subcutaneously. Thus, tumor cells could be labeled by RFP. [18F]-Fluorodeoxyglucose ([18F]-FDG) was used as radioactive tracers of PET imaging. The capacity of this hybrid system for tumor detection would be confirmed by the results of this new designed *in vivo* experiment.

2. Materials and Methods

2.1. *Experimental setup*

Figure 1 shows the schematic diagram of the system. The PET and FMT modules are mounted orthogonally with centers of the CCD camera and PET detectors at the same height. A rotary stage, which is used to produce projection data of different angles, is located in the center of two modules. Mouse is hung on the stage vertically with limbs suspended by clamps. The whole system is controlled by specially developed software to perform dual-modality simultaneous data acquisition.

A full-angle free-space FMT system is used to acquire fluorescent signals in the dual-modality system. As shown in Fig. 1, a 250 W Halogen lamp (7ILT250, 7-star, Beijing, China), with wavelength ranging from 300 to 2,500 nm is employed as the excitation light source. With a piece of band-pass filter, it can provide light with specific wavelength. Then the light travels through an optical fiber and a collimator lens in succession. The collimator lens is used to generate uniform excitation beam and is placed next to the CCD camera. A back-illuminated cooled CCD camera (Andor, Belfast, Northern Ireland, UK) coupled with a 35 mm f/1.4 lens (Pentax, Hoya, Japan) is selected to capture photons produced by fluorescent dyes. The pixel number of the image acquired by the CCD is 512×512 at most. Another band-pass filter is positioned in front of CCD for fluorescent signal acquisition.[9]

As to PET module, a pair of planar detectors is designed to record γ rays from the positronium annihilation. Each panel detector consists of four blocks and each block has 16×16 cerium-doped lutetium yttrium orthosilicate (LYSO) crystals arranged in square. The size of each crystal is $1.9 \times 1.9 \times 10\,\text{mm}^3$. To improve light collection efficiency, each crystal is wrapped with reflective material, which results in detector pixel size of $2.0 \times 2.0 \times 10\,\text{mm}^3$. The whole sensitive area of each detector is $64 \times 64\,\text{mm}^2$. To effectively avoid dead area, pyramid-like light guide is used to couple position sensitive photo multiply tubes (PSPMT) and panel detector in the pattern of each PSPMT to one block. A position lookup table based on flood histogram of the block detector is used to determine which crystal the γ ray is incident with. Besides, a digital signal processing unit (DSPU) is designed to process events information from detectors. The DSPU is encapsulated in a Compact-PCI (CPCI) enclosure and the data is transferred to PC via local area network (LAN).[8]

2.2. *Reconstruction and fusion algorithms*

PET and fluorescent data are processed separately before fusion. The list-mode PET data is converted to sinogram mode according to their labeled angles. Data after conversion consists of 512 projections,

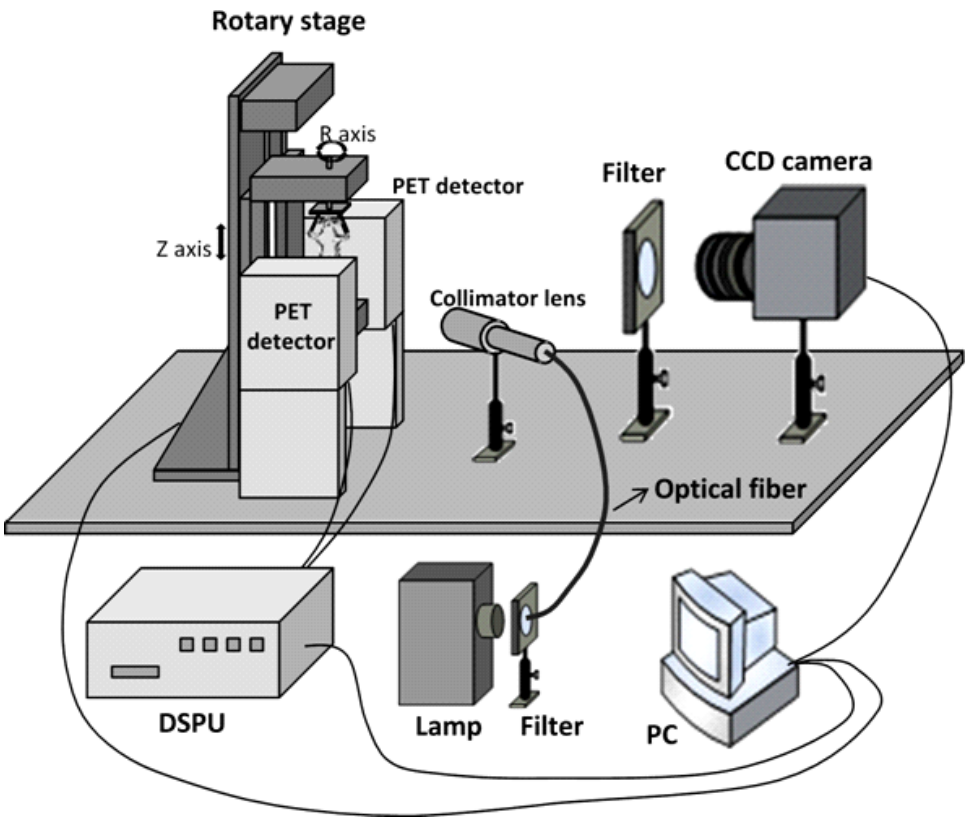

Fig. 1. Schematic diagram of the whole system. The optical module includes a tungsten halogen lamp, an optical fiber, a collimator lens, two band-pass filters, a lens and a CCD camera. The PET module mainly includes two planar detectors and a digital signal processing unit (DSPU).

and every projection is a histogram. Afterwards, Fourier rebinning (FORE) method is employed to rebin the 3D histogram-mode to 2D. Finally, filtered back projection (FBP) and 2D ordered subset expectation maximization (OSEM) methods are used to reconstruct the 3D radionuclide distribution.[8,10]

As to fluorescent imaging, the photon propagation is always modeled using the diffusion equation coupled with Robin-type boundary condition.

$$\begin{cases} -\nabla \cdot [D(r)\nabla\Phi(r)] + \mu_a(r)\Phi(r) = s_0(r) & r \in \Omega, \\ \Phi(r) + 2D(r)q\dfrac{\partial\Phi(r)}{\partial\vec{n}} = 0 & r \in \partial\Omega, \end{cases} \tag{1}$$

where $D(r) = 1/(3\mu'_s(r))$ is the diffusion coefficient at position r, $\mu'_s(r)$ is the reduced scattering coefficient, and $\mu_a(r)$ is the absorption coefficient. Ω is the domain of the imaged object with a boundary of $\partial\Omega$, q is a constant depending on the optical refractive index mismatch on the boundary, and $\vec{n}$ denotes the outward normal vector of the boundary $\partial\Omega$.

With the method of finite elements method (FEM), we produce the following weight matrix from the diffusion equation,

$$WX = \Phi, \tag{2}$$

where W is the matrix weight, each element W_{ij} in the matrix means the contribution of jth voxel of the discrete element to the measurement due to the ith source-detector pair. Finally, the unknown fluorescent probe distribution X is reconstructed by solving Eq. (2) with algebraic reconstruction technique (ART).[9,12] Typical iteration number in the paper is 50.

Co-registration is needed before data fusion. Herein, because fluorescent and PET data are acquired simultaneously, there is no distraction of the mouse body. We use rigid registration method for co-registration. As to fusion, independent color bars are provided. Corresponding voxels of both data are found to be blending and displayed simultaneously.

2.3. *Imaging protocol*

A tumor-bearing BALB/c-nu mouse (female) was chosen as the research object for *in vivo* validation of the dual-modality system. RFP genes were previously transduced into MD-MB-231 breast cancer cells. About seven days before the experiments, the mouse was injected subcutaneously at the right lower abdomen with a single dose of 10^6 tumor cells that could express RFP. The tumor was about 0.3 cm^3 when the experiments were performed.

For RFP fluorescence detection, 525 nm excitation filter (525AF50, Caliper Life Sciences, MA, US) and DsRed emission filter (575−650 nm, Caliper Life Sciences, MA, US) were utilized. Because visible light attenuates a lot in mouse tissues, reflective illumination mode, which is usually used for planar imaging, is adopted to get fluorescent signals. That is, we combine reflective illumination with full-angle data acquisition mode together.

[18F]-FDG was employed as the radioactive tracer for PET imaging. After the mouse was anesthetized by isoflurane, 1.5 mCi [18F]-FDG was injected through tail vein. One hour was needed to wait before imaging, ensuring [18F]-FDG is distributed throughout the whole body.

During the whole simultaneous acquisition, the stage would rotate 720° in total. During the first 360° rotation, 512 projections of PET were acquired every 0.7° and 64 projections of fluorescent data were acquired every 5.625°. That is, each fluorescent projection was acquired after every eight PET projections. Acquisition time for each projection of PET and FMT data was 2 and 0.3 s, respectively (CCD electron multiplier gain (EM) is 8). The second 360° rotation was used to get 72 white-light surface images, which were used to reconstruct the contour of the mouse. Exposure time for each projection was usually 0.01 s (EM = 0). The total acquisition time for one experiment was about 20 min.

3. Results

In the following, we present reconstructed results for PET and fluorescent imaging. PET results have the dimensions of $128 \times 128 \times 63$ with pixel size of $0.5 \times 0.5 \times 1\,mm^3$. Fluorescent results have the dimensions of $45 \times 45 \times 53$ with pixel size of $0.5 \times 0.5 \times 0.5\,mm^3$. Results of two modules are then fused.

Figure 2 shows fluorescent projection images collected at two typical angles (90° and 180°). In Figs. 2(a) and 2(b) the white-light images at different angles are seen. Red arrows indicate where the tumor is located. Figures 2(c) and 2(d) show the white-light images fusing with fluorescent signals. We can find that fluorescent signals at right lower abdomen (red arrows), which indicates where the tumor is located.

Figure 3 shows the reconstructed 3D images of the results of the mouse. Figure 3(a) displays distribution of RFP with contour of the mouse (2.7 cm height of the mouse is displayed). Figure 3(c) is the 3D-reconstructed image of PET data, which shows the metabolic information of FDG (6.3 cm height of the mouse is displayed). To reflect details of the reconstructed results, tomographic images in Figs. 3(b) and 3(d) are showcased respectively. In Fig. 3(b), the location of tumor can be easily recognized (indicated by the black arrow). Meanwhile, Fig. 3(d) reveal metabolic information of the tumor (indicated by the green arrow). There are high radionuclide intensities beside the tumor area. That is because the location of the tumor is near the bladder, where radioactive tracers accumulate in *in vivo* experiments.

Finally, 3D-fluorescent reconstruction results are fused with PET results. In Fig. 4, the coronal (left), sagittal (right), and transverse (bottom) plane of the 3D-fused results are shown. Independent color bars are provided for PET and FMT data. For PET results, metabolic information of the whole body is offered. Usually, tumor cells have more active metabolism than normal tissues, corresponding to higher radioactive signals. However, because there are high accumulation of FDG in some organs (e.g., heart, bladder), it is difficult to determine the tumor area. FMT results indicate the tumor location exactly whereas the molecular information of tissues around the tumor is ignored. Although both modalities can offer molecular information, they are complementary rather than overlapping. After fusion, radioactive and fluorescent information is displayed simultaneously. From Fig. 4, we find that the tumor is at right lower abdomen, which is in accordance with the real location. Moreover, fused results show metabolic information of FDG in and around the tumor, which provides useful information for tumor research.

4. Discussion and Conclusion

The experiment presented here is devoted to assess the feasibility and performance of the combined

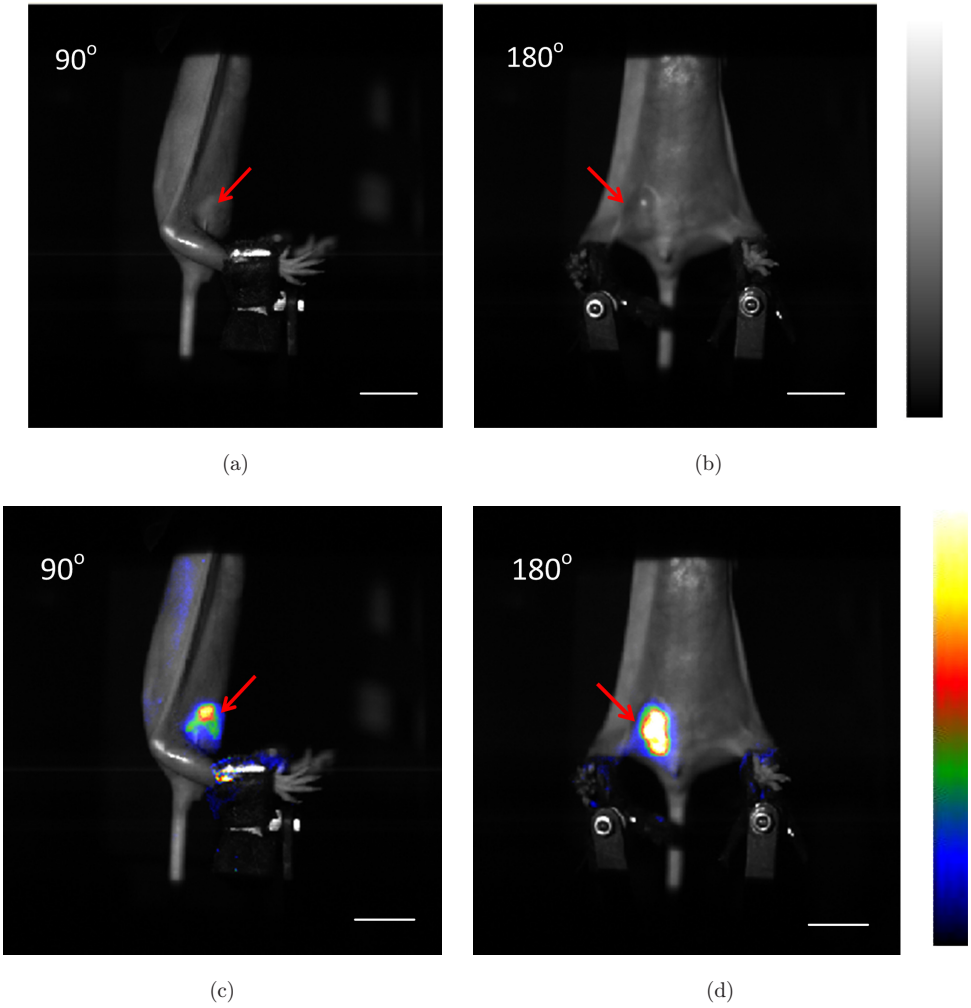

(a) (b)

(c) (d)

Fig. 2. Fluorescent projection images of the mouse at different angles. (a), (b) White-light mouse images. (c), (d) White-light images fusing with fluorescent signals. Red arrows indicate where the tumor is located. Scale bars represent 1 cm.

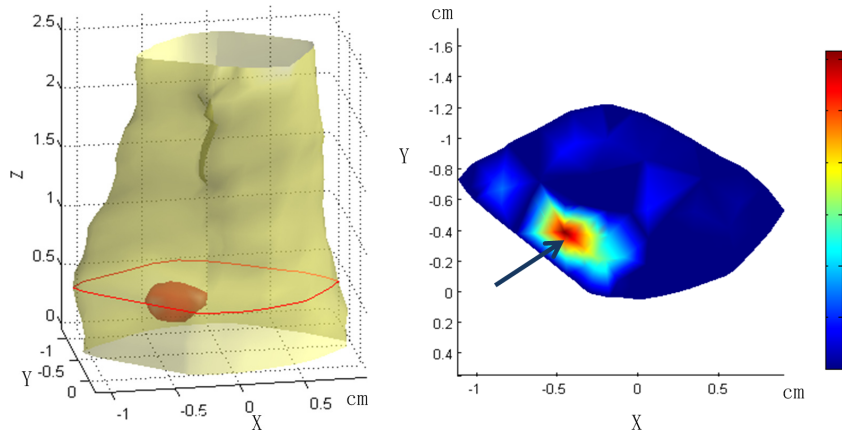

(a) (b)

Fig. 3. Reconstructed results of two modalities. (a), (c) Fluorescent and PET reconstructed results, respectively. 3D fluorescent results in (a) are showed with a threshold of 60% of the maximum value. (b) Tomographic fluorescent image at the height is demonstrated by the red curve in (a). (d) Tomographic PET image is at the same height as (b). Arrows in (b) and (d) indicate where the tumor is located.

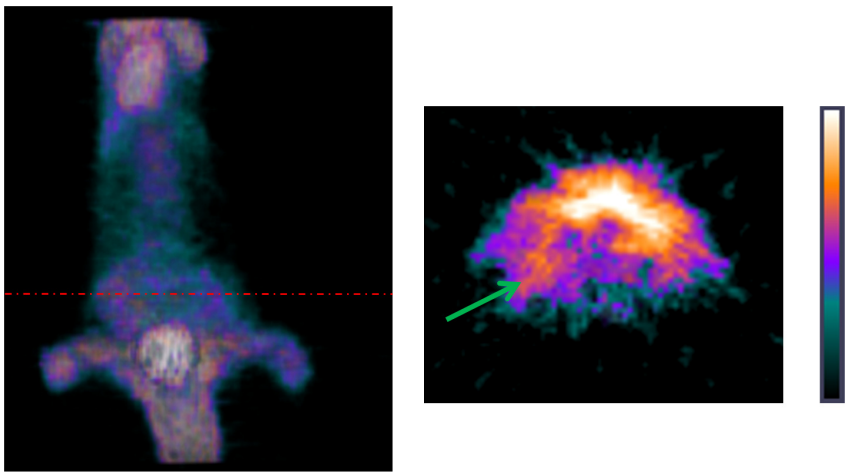

(c) (d)

Fig. 3. (*Continued*)

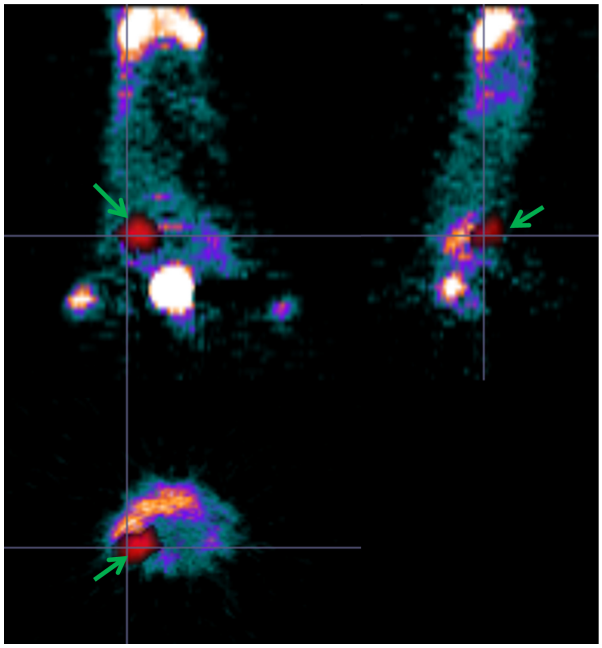

Fig. 4. 3D fusion images of FMT and PET. The coronal (left), sagittal (right), and transverse plane (bottom) of the fused 3D-reconstruction images are showed. Red parts of the images, indicated by green arrows, represent fluorescent data. PET result provides FDG metabolic information in the tumor.

PET and FMT system. Different imaging modalities may supply different information for *in vivo* imaging that could determine improvements on oncological investigations. For example, in Fig. 3(a), FMT results show exactly where the tumor is located, which cannot be distinguished in PET results (Fig. 3(e)). However, the PET results reveal metabolic information near the tumor area, which is valuable in tumor diagnosis. After fusion, we can get complementary information of the tumor clearly than single modality alone.

Since both modalities offer functional information rather than anatomical information and resolutions of both images are not very high, future work is needed in reconstruction algorithms to improve image quality. The reconstructed results are co-registered with rigid registration method before fusion. It is simpler but less competent to complicated conditions compared to non-rigid registration ones. However, because relative positions of detectors are fixed and data acquisition is simultaneous, there are fewer difficulties with registration. That is, the system has accomplished most of the work for registration, which is an advantage of combined system. More efforts are needed to be spent on fusing information of both modalities.

In the experiment, RFP is used as the fluorescent probes for tumor investigation. Because RFP is expressed by transduced genes of tumor cells, it can indicate tumor cells specifically. This is more effective and convincing than non-specific fluorescent dyes. Moreover, in recent years, elegant probes have been developed rapidly. One trend is to fuse signaling moieties of two modalities into one molecule (monomolecular multimodal imaging agents), avoiding the increase in the potential for cumulative toxicity and complicating data fusion.[13] For example, Schipper and colleagues have successfully developed a QD-based nano-probe for dual PET

and NIRF imaging of tumor vascular endothelial growth factor receptor expression.[14]

In summary, we performed an *in vivo* experiment with the combined PET and FMT system. Results validated the feasibility of the system for the *in vivo* application and showed its superiority to single-modality imaging alone. With more future efforts, it will play an important role in researches on tumor diagnosis, drug development and metabolism of complex bioprocess.

Acknowledgments

The authors would like to thank X. Zhang, faculty of XinAoMDT Technology Co., Ltd., for the work of system software development. This work is supported by the National Natural Science Foundation of China under Grant Nos. 81071191, 60831003, 30930092, 30872633; the Tsinghua-Yue-Yuen Medical Science Foundation; the National Basic Research Program of China (973) under Grant No. 2011CB707701.

References

1. M. S. Judenhofer, H. F. Wehrl, D. F. Newport, *et al.*, "Simultaneous PET-MRI: A new approach for functional and morphological imaging," *Nat. Med.* **14**(4), 459−465 (2008).
2. G. A. Kastis, L. R. Furenlid, D. W. Wilson, *et al.*, "Compact CT/SPECT small-animal imaging system," *IEEE Trans. Nucl. Sci.* **51**, 63−67 (2004).
3. P. M. Winter, A. M. Morawski, S. D. Caruthers, *et al.*, "Molecular imaging of angiogenesis in early-stage atherosclerosis with $\alpha v\beta 3$-integrin-targeted nanoparticles," *Circulation* **108**, 2270−2274 (2003).
4. N. Deliolanis, T. Lasser, D. Hyde, *et al.*, "Free-space fluorescence molecular tomography utilizing 360° geometry projections," *Opt. Lett.* **32**(4), 382−384 (2007).
5. M. Autiero, L. Celentano, R. Cozzolino, *et al.*, "Experimental study on *in vivo* optical and radionuclide imaging in small animals," *IEEE Trans. Nucl. Sci.* **52**(1), 205−209 (2005).
6. D. L. Prout, R. W. Silverman, A. Chatziioannou, "Detector concept for OPET-A combined PET and optical imaging system," *IEEE Trans. Nucl. Sci.* **51**(3), 752−756 (2004).
7. J. Peter, D. Unholtz, R. B. Schulz, *et al.*, "Development and initial results of a tomographic dual-modality positron/optical small animal imager," *IEEE Trans. Nucl. Sci.* **54**, 1553−1560 (2007).
8. S. Liu, B. Zhang, X. Wang, *et al.*, "A dual-modality system for simultaneous FMT and PET tomographic imaging of small animals," *IEEE Trans. Nucl. Sci.* **58**(1), 51−57 (2011).
9. F. Liu, X. Liu, D. Wang, *et al.*, "A parallel excitation based fluorescence molecular tomography system for whole-body simultaneous imaging of small animals," *Ann. Biomed. Eng.* **38**(11), 3440−3448 (2010).
10. H. M. Hudson, R. S. Larkin, "Accelerated image reconstruction using ordered subsets of projection data," *IEEE Trans. Med. Imag.* **13**(4), 601−609 (1994).
11. X. Liu, D. Wang, J. Bai, "Fluorescence molecular tomography with optimal radon transform based surface reconstruction," *31st Annu. Int. Conf. Proc. IEEE Engineering Medical Science*, Minnesota, pp. 1404−1407 (2009).
12. X. Song, D. Wang, J. Bai, "Reconstruction for free-space fluorescence tomography using a novel hybrid adaptive finite element algorithm," *Opt. Express* **15**(26), 18,300−18,317 (2007).
13. J. Culver, W. Akers, S. Achilefu, "Multimodality molecular imaging with combined optical and SPECT/PET modalities," *J. Nucl. Med.* **49**, 169−172 (2008).
14. M. L. Schipper, Z. Cheng, S. W. Lee, *et al.*, "MicroPET-based biodistribution of quantum dots in living mice," *J. Nucl. Med.* **48**, 1511−1518 (2007).